Tréhu, A.M., Bohrmann, G., Torres, M.E., and Colwell, F.S. (Eds.)
Proceedings of the Ocean Drilling Program, Scientific Results Volume 204

14. Data Report: $^{129}I/I$ Ratios and Halogen Concentrations in Pore Water of Hydrate Ridge and Their Relevance for the Origin of Gas Hydrates: A Progress Report[1]

Udo Fehn,[2] Zunli Lu,[2] and Hitoshi Tomaru[2]

ABSTRACT

We report iodine and bromine concentrations in a total of 256 pore water samples collected from all nine sites of Ocean Drilling Program Leg 204, Hydrate Ridge. In a subset of these samples, we also determined iodine ages in the fluids using the cosmogenic isotope ^{129}I ($T_{1/2}$ = 15.7 Ma). The presence of this cosmogenic isotope, combined with the strong association of iodine with methane, allows the identification of the organic source material responsible for iodine and methane in gas hydrates. In all cores, iodine concentrations were found to increase strongly with depth from values close to that of seawater (0.0004 mM) to concentrations >0.5 mM. Several of the cores taken from the northwest flank of the southern summit show a pronounced maximum in iodine concentrations at depths between 100 and 150 meters below seafloor in the layer just above the bottom-simulating reflector. This maximum is especially visible at Site 1245, where concentrations reach values as high as 2.3 mM, but maxima are absent in the cores taken from the slope basin sites (Sites 1251 and 1252). Bromine concentrations follow similar trends, but enrichment factors for Br are only 4–8 times that of seawater (i.e., considerably lower than those for iodine).

Iodine concentrations are sufficient to allow isotope determinations by accelerator mass spectrometry in individual pore water samples collected onboard (~5 mL). We report $^{129}I/I$ ratios in a few samples from

[1] Fehn, U., Lu, Z., and Tomaru, H., 2006. Data report: $^{129}I/I$ ratios and halogen concentrations in pore water of Hydrate Ridge and their relevance for the origin of gas hydrates: a progress report. *In* Tréhu, A.M., Bohrmann, G., Torres, M.E., and Colwell, F.S. (Eds.), *Proc. ODP, Sci. Results*, 204, 1–25 [Online]. Available from World Wide Web: <http://www-odp.tamu.edu/publications/204_SR/VOLUME/CHAPTERS/107.PDF>. [Cited YYYY-MM-DD]
[2] Department of Earth and Environmental Sciences, University of Rochester, Rochester NY 14627, USA. Correspondence author: **fehn@earth.rochester.edu**

Initial receipt: 26 January 2005
Acceptance: 28 June 2005
Web publication: 16 January 2006
Ms 204SR-107

each core and a more complete profile for one flank site (Site 1245). All $^{129}I/I$ ratios are below the marine input ratio ($R_i = 1500 \times 10^{-15}$). The lowest values found at most sites are between 150 and 250 $\times$ 10^{-15}, which correspond to minimum ages between 40 and 55 Ma, respectively. These ages rule out derivation of most of the iodine (and, by association, of methane) from the sediments hosting the gas hydrates or from currently subducting sediments. The iodine maximum at Site 1245 is accompanied by an increase in $^{129}I/I$ ratios, suggesting the presence of an additional source with an age younger than 10 Ma; there is indication that younger sources also contribute at other sites, but data coverage is not yet sufficient to allow a definitive identification of sources there. Likely sources for the older component are formations of early Eocene age close to the backstop in the overriding wedge, whereas the younger sources might be found in recent sediments underlying the current locations of the gas hydrates.

INTRODUCTION

Hydrate Ridge is the location of unusually high concentrations of gas hydrates and was the site of Ocean Drilling Program (ODP) Leg 204 in the summer of 2002. It is located on the Oregon (USA) continental margin and is part of the accretionary complex formed by the subduction of the Juan de Fuca plate under the North American plate. The large concentrations of gas hydrates in this area make derivation of methane from local sources rather unlikely and raises questions about the potential source formations and pathways for the hydrocarbons and associated water. Because of the strong affiliation of iodine with organic material, together with the presence of a cosmogenic isotope, the iodine isotopic system is a powerful tool to determine source formations responsible for the release of hydrocarbons. We present here results of iodine and bromine determinations in a large set of pore water samples from all cores taken during Leg 204, as well as first results for $^{129}I/I$ ratios in a subset of these samples.

THE IODINE SYSTEM

As a strongly biophilic element, iodine is commonly found heavily enriched in fluids associated with hydrocarbons, such as oil field brines (Moran et al., 1995) or coal-bed methane reservoirs (Snyder et al., 2003). Concentrations are particularly high in pore water associated with gas hydrates, where iodine is enriched typically by factors of 500 or more compared to seawater (Martin et al., 1993; Egeberg and Dickens, 1999; Fehn et al., 2003). The strong association between iodine and methane is not restricted to gas hydrate sites but is also observed in other methane-rich fluids in forearc settings (Muramatsu et al., 2001) or coal-bed methane reservoirs (Snyder et al., 2003). This association strongly suggests that these two compounds are derived from the same organic source and that the iodine system can be used to identify the formations responsible for the release of these two compounds. Accordingly, the iodine isotopic system has been used recently for the determination of source formations of hydrocarbons in a variety of settings, including investigations of gas hydrate occurrences at Blake Ridge (Fehn et al., 2000), Nankai Trough (Fehn et al., 2003), and the Peru margin (Fehn et al., in press).

Iodine has one stable isotope, ^{127}I, and one long-lived radioisotope, ^{129}I. ^{129}I is a member of a group commonly called cosmogenic isotopes because they are produced mostly or partially by the interaction of cosmic rays with atoms of the atmosphere. It has the longest half-life ($T_{1/2}$ = 15.7 Ma) of the radioisotopes in this group and is produced by the spallation of Xe isotopes in the atmosphere and by spontaneous fission of ^{238}U in the crust. Both of these processes contribute similar amounts of natural ^{129}I to surface reservoirs (Fabryka-Martin et al., 1985). Iodine moves quickly through most surface reservoirs, and natural iodine is isotopically homogeneous at the surface of the Earth, including oceans, shallow sediments, and the biosphere. The exchange between marine and terrigenous sources is sufficiently rapid to have an isotopically well mixed signal in surface reservoirs at the resolution available for natural ^{129}I concentrations. Preanthropogenic $^{129}I/I$ ratios therefore provide identical age dependence for marine and terrigenous sources, although terrigenous sources typically have lower iodine concentrations. Anthropogenic ^{129}I is a third component present in surface reservoirs and is related to releases from weapons tests and reprocessing plants. The widespread occurrence of anthropogenic ^{129}I in rivers and lakes throughout the world is evidence for the high mobility of this element on a global scale (Santschi and Schwehr, 2004; Snyder and Fehn, 2004). Although the current isotopic equilibrium in surface reservoirs has been substantially disturbed because of this contribution (e.g. Schink et al., 1995; Moran et al., 1999; Oktay et al., 2001), the influence of anthropogenic ^{129}I is mostly restricted to the zone of bioturbation (Fehn et al., 1986; Moran et al., 1998), with minor penetration possible beyond that zone as observed in the Gulf of Mexico (Oktay et al., 2000).

Because iodine has only one stable isotope, ^{127}I, its isotopic composition is reported as $^{129}I/I$. The long residence time (300,000 yr) of iodine in the oceans (Broecker and Peng, 1982) provides a homogeneous isotopic signal in the marine system. Recent sediments below the zone of bioturbation (i.e., without the presence of anthropogenic I) have $^{129}I/I$ ratios of $R_i = (1500 \pm 150) \times 10^{-15}$ (Fehn et al., 1986; Moran et al., 1998). Ratios supporting this value were also found in determinations of preanthropogenic seawater and algae (e.g., Schink et al., 1995; Cooper et al., 1998; Y. Muramatsu, unpubl. data, 2002). This ratio, which is used as starting value for ^{129}I-based age calculations, is two orders of magnitude above the detection limit of accelerator mass spectrometry (AMS), the method of choice for the detection of cosmogenic radioisotopes. The half-life of ^{129}I, together with the observed input ratios and the detection limit for $^{129}I/I$ (2×10^{-14}) (Sharma et al., 2000), allows applications of this dating method within a range of ~80 m.y. The calculation of iodine ages t_{min} from a measured ratio R_m uses the following equation, with $\lambda_{129} = 4.41 \times 10^{-8}$/yr being the decay constant of ^{129}I:

$$t_{min} = \ln (R_m/R_i)/(-\lambda_{129}). \quad (1)$$

Depending on the geologic situation, a correction for the contribution of fissiogenic ^{129}I has to be taken into account. The addition of fissiogenic ^{129}I is a function of age and uranium concentration of the host formation and the probability of transport from host formation into the fluids. Although the addition of fissiogenic ^{129}I presents an uncertainty for the ages calculated, the potential correction in the age range found here is probably <5 m.y. in the oldest samples found. Because the presence of either fissiogenic or anthropogenic ^{129}I would have raised

the measured ratio, ages calculated from equation 1 are minimum ages. The presence of anthropogenic ^{129}I typically increases the ratio beyond the preanthropogenic input value and is an unlikely presence in marine sediments beyond the layer of bioturbation (Fehn et al., 1986; Moran et al., 1998), but it can play a role in samples taken from open systems on land.

Concentrations of iodine in surface fluids are generally low, 0.4 µM (55 ppb) in seawater (Geochemical Reference Model, **earthref.org/GERM**) and <0.02 µM in freshwater (e.g., Moran et al., 1999), depending in part on the presence of organo-iodine compounds (Schwehr and Santschi, 2004). Associated with organic material, iodine can be considerably enriched: typical concentrations in oil field brines are ~80 µM (e.g. Moran et al., 1995), and concentrations as high as 2 mM were found in pore water associated with gas hydrates (Egeberg and Dickens, 1999) and in methane-rich cold seeps of forearc areas (Muramatsu et al., 2001). Molecular diffusion coefficients depend on the speciation of iodine and vary between 1.08×10^{-5} cm^2/s for iodate and 2.05×10^{-5} cm^2/s for iodide, bracketing the value for methane (1.49×10^{-5} cm^2/s), but are much lower for organo-iodine compounds (all values for 25°C are from Linde, 2004). Because the predominant iodine species in deep, methane-rich fluids is iodide (Muramatsu et al., 2001), the similarity of diffusion coefficients suggests that methane and iodine travel together in fluids. This statement applies as long as methane does not convert into the gas phase, a situation that might occur in and below the gas hydrate stability zone (Torres et al., 2004).

The investigation of iodine concentrations and isotope ratios is accompanied by a study of bromine and chloride concentrations. Of the three halogens investigated here, iodine has the strongest biophilic character, chlorine has little association with organic material, and the association of bromine with organic matter falls in between those two characteristics. Concentrations of chlorine in pore water associated with gas hydrates typically are at or somewhat below that of seawater, often accompanied by freshening in the layer just above the bottom-simulating reflector (BSR). This observation is commonly related to the release of water due to the dissolution of gas hydrate crystals and is used for the quantification of the amount of gas hydrates at a given location (e.g., Ussler and Paull, 2001; Tomaru et al., 2004). In several gas hydrate locations, chlorine concentrations decrease consistently with depth, suggesting an influx of deep waters with Cl concentrations below that of seawater (Ussler and Paull, 2001; Hesse, 2003). Chlorine has also a cosmogenic isotope (^{36}Cl; $T_{1/2}$ = 0.3 Ma), but because of the high concentration of "dead" Cl in seawater the ratio, $^{36}Cl/Cl$ is below the detection limit of AMS. Chlorine also has two stable isotopes, ^{35}Cl and ^{37}Cl, and their ratio has recently been used for the detection of sources of fluids in gas hydrate settings (e.g., Hesse, 2003). Studies of this kind have not been carried out for Hydrate Ridge so far.

Bromine concentrations follow a pattern similar to that of iodine but with considerably lower enrichment factors (e.g., Egeberg and Dickens, 1999). Element ratios are useful for the determination of the origin of fluids (e.g., Frape et al., 2004) and of the organic source material (Muramatsu et al., 2001), and they therefore complement the observations based on concentrations or isotope ratios.

GEOLOGIC SETTING

Hydrate Ridge is part of the Cascadia accretionary complex, which is formed by the oblique subduction of the Juan de Fuca plate beneath the North America plate (Fig. F1A). The current subduction rate is ~4.5 cm/yr (Tréhu, Bohrmann, Rack, Torres, et al., 2003), with an age of <10 Ma identified for the Juan de Fuca slab (Jarrard, 1986). A deformation front is observed ~100 km west of the coast and is considered the seaward edge of the Cascadia subduction zone. Landward to the deformation front is the subduction complex, which is composed of highly deformed marine sediments of Pliocene to Miocene age (Snavely and Wells, 1996). The Siletz terrane, a basaltic formation of Paleocene to early Eocene age, forms the backstop to the accretionary complex and the basement to much of the Cascadia forearc. The boundary between the Siletz terrane and the accretionary complex is obscured by high-velocity rocks that appear in seismic surveys in the lower continental crust beneath the coastline and extend to the top of the descending slab ~20 km offshore (Parsons et al., 1998). The origin of this high-velocity body is unknown. Snavely (1987) mapped this contact and suggested that the western boundary of the Siletz terrane is an Eocene-age strike-slip fault 30 km west of the coastline, called the Fulmar fault, which coincides with the location of the edge of the high-velocity body. The Fulmar fault is also thought to be the western boundary of the marginal rift basin that is filled by a sequence of siltstone, turbidite sandstone, and conglomerate of early Eocene age. The bottom of the basin is mostly Paleocene to lower Eocene basalt. The Siletz volcanic highs and overlying marine sedimentary rocks were deformed by the subduction of the Kula-Farallon plate at ~52 Ma (Snavely and Wells, 1996). The complicated tectonic and depositional history of the Cascadia margin is reflected in numerous faults, mostly dipping from west to east (Snavely, 1987; Snavely and Wells, 1996). Some prominent faults dipping in the opposite direction have been identified in the western flank region of Hydrate Ridge, apparently related to the most recent tectonic events in this area (Johnson et al., 2003; **Chevallier et al.,** this volume). Figure F1B is a highly simplified cross section through the Cascadia margin, illustrating schematically the age relations in this region (after Snavely, 1987; Snavely and Wells, 1996).

Hydrate Ridge itself is 25 km long and 15 km wide, trending roughly north–south, and is subdivided into the northern and southern summits. Water depths along the ridge are ~1000 m with the summits reaching depths of 600 and 800 m, respectively. The ridge is covered by sandy and silty marine sediments of Quaternary age. Gas hydrates are ubiquitous throughout the entire ridge, indicated by nearly continuous BSRs and the presence of massive hydrate deposits at the top of the southern summit (Tréhu et al., 1999; Tréhu, Bohrmann, Rack, Torres, et al., 2003). U-Th data of seafloor carbonates suggest that gas hydrates on the southern summit are somewhat younger than those on the northern summit (Teichert et al., 2003). The ridge has been the site of numerous investigations, the latest of which was Leg 204 (Tréhu, Bohrmann, Rack, Torres, et al., 2003), focusing on the southern summit. The nine drill sites (Fig. F2) reached depths between 150 and 440 meters below seafloor (mbsf). We report here results for all nine sites, which we have subdivided for further discussion into flank sites (1244–1248), summit sites (1249–1250), and slope basin sites (1251–1252). Based on the iodine results, we group Site 1244 with the flank sites, deviating slightly

F1. Tectonic setting and west–east cross section, p. 16.

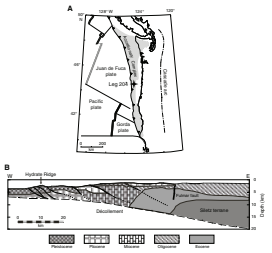

F2. Distribution of drill sites, p. 17.

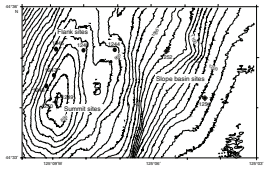

from the grouping suggested in Tréhu, Bohrmann, Rack, Torres, et al. (2003), where it is listed among the slope basin sites.

SAMPLES AND METHODS

We received a total of ~260 pore water samples of 5–10 mL each sealed in glass containers from all sites drilled during Leg 204. Pore water was extracted from whole-round cores of 10–25 cm length, usually sampled soon after core recovery. These sediment cores were skinned off to remove potential seawater contamination during drilling and were squeezed with Manheim-type squeezers following the ODP sampling protocol for the extaction of pore water (Tréhu, Bohrmann, Rack, Torres, et al., 2003). Dissolved chloride concentration was measured by triplicate titration with silver nitrate ($AgNO_3$) on board ship with precisions better than 0.4%; the values were corrected for the presence of the other halogens assuming seawater ratios (Torres et al., 2004). Total iodine and bromine concentrations were measured by inductively coupled plasma–mass spectrometry, using the Thermal X7 instrument at the University of Rochester (New York, USA). We followed established methods (Muramatsu and Wedepohl, 1998), except for replacing nitric acid with a tertiary amine solution (Spectrasol CFA-C), which was added to the solution matrix to prevent precipitation in the tubing. A washout time of 2 min was found to be sufficient to allow the signal to return to background levels. Accuracies for concentration values of iodine and bromine are better than 1% and are not reported individually.

A major goal of this investigation is the determination of $^{129}I/I$ ratios in the pore water samples. So far, $^{129}I/I$ ratios have been measured on a subset of 41 samples selected from all 9 sites. Iodine was extracted and precipitated as AgI at the Rochester Cosmogenic Isotope Laboratory (New York, USA), using methods outlined in Fehn et al. (1992). The relatively high iodine concentrations in the samples allowed preparation of AMS targets from individual pore water samples. The actual AMS determinations were carried out at PrimeLab, Purdue University (Indiana, USA), again following established routines (Sharma et al., 2000). Individual accuracies of the AMS determinations (1σ) are listed together with the ratios. The actual accuracy of a determination reflects the stability of the AMS system as well as the amount of sample material provided. About 1 mg of AgI is sought for an actual AMS determination, but ratios have been determined with amounts as low as 0.1 mg of AgI, although with diminished accuracy.

RESULTS

Halogen Concentrations

Iodine and bromine concentrations were determined at all nine drill sites; results are listed in Table T1, together with the chloride results from the shipboard measurements (Tréhu, Bohrmann, Rack, Torres, et al., 2003). Except for samples very close to the seafloor, concentrations for iodine fall into a range between 0.5 and 2.3 mM, constituting enrichments by factors up to 5000 compared to seawater (0.0004 mM) (Geochemical Reference Model, earthref.org/GERM). A strong increase in iodine concentrations with depth is visible in all profiles at Hydrate Ridge (Fig. F3). Although some sites reach rather constant values

T1. Concentrations of iodine, bromine, and chlorine, p. 23.

F3. Depth profiles for iodide, bromide, and chloride, p. 18.

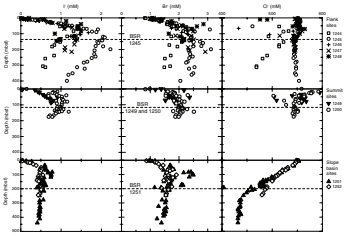

quickly with depth, several of the sites display maxima in iodine concentrations at depths between 100 and 150 mbsf (i.e., in the layer above the BSR). This maximum is clearly visible at the flank sites, most pronounced at Site 1245, and is probably also present at the summit sites, although the drilling depths there are not sufficient to make a definitive statement. Together with generally lower concentrations, the two sites in the slope basin do not have maxima comparable to those at the flank sites.

Bromine concentrations follow patterns similar to that of iodine concentrations, with concentrations falling into a range only slightly higher than that of iodine. Because the bromine concentration in seawater (0.8 mM) (Geochemical Reference Model, **earthref.org/GERM**) is considerably higher than that of iodine, enrichment factors are much lower for Br than for I. Maxima in bromine concentrations are also present at depths just above the BSR but are not as strongly pronounced as in iodine. Chlorine concentrations follow a very different pattern from that of the other two halogens. For most of the sections, Cl^- concentrations are close to that of seawater (550 mM), with some scatter in the sections just above the BSR. Several of the cores display a distinct decrease in Cl^- concentrations, particularly discernable at the slope basin sites. At a few summit sites, Cl^- concentrations are greatly enhanced very close to the sediment/seawater interface, reaching values >1000 mM at Site 1249. No comparable increase is observed for iodine or bromine concentrations in this depth range, but it is worth mentioning that, because of the goals of our investigation, coverage of this depth range was very limited in our sample set.

The general observations for halogen concentrations are in good agreement with those found for other gas hydrate locations, such as investigations at the Peru margin (Martin et al., 1993), Blake Ridge (Egeberg and Dickens, 1999), or Nankai Trough (Fehn et al., 2003). At all of these locations, very strong enrichment of iodine is observed together with parallel enrichment of bromine. Whereas all of these sites have iodine concentrations of 0.2 mM or higher (i.e., are enriched by factors of 500 or more compared to seawater), pore water in sediments without gas hydrates have iodine concentrations of ~0.001 mM (Martin et al., 1993). Although the general enrichment in iodine at Hydrate Ridge is similar to other gas hydrate sites, the specific characteristics differ both in degree of enrichment and shape of depth profiles from the other sites. The maximum concentration measured at Site 1245 (2.3 mM) is the highest iodine concentration found at gas hydrate sites so far. Although concentrations at the other Leg 204 sites are somewhat lower, they still are among the highest values observed at gas hydrate locations. Maxima in iodine concentrations comparable to those found at the flank sites have, so far, not been observed at sites other than Hydrate Ridge. As at other gas hydrate sites, chlorine concentrations show very different behavior from that of the other two elements; specifically, concentrations of Cl^- are at or below that of seawater and show considerable scatter in the layers above the BSR.

Although the general characteristics of halogens at Hydrate Ridge sites are within the range of observations found at other gas hydrate sites, there are important differences among the sites from Leg 204, specifically between the flank sites and the slope basin sites. The degree of enrichment in iodine, as well as the presence of maxima at the flank sites (and perhaps at the summit sites), is different from the observations for the slope basin sites. Profiles at the slope basin sites and Site 1244 of the flank sites show a consistent decrease in Cl^- concentrations

with depth, in considerable contrast to the other sites on the flank and summit. Because a decrease of this type might be related to the influx of deep fluids, as suggested for other gas hydrate sites (e.g., Hesse, 2003), this observation might suggest different hydrologic regimes for separate parts of Hydrate Ridge.

As is typical for gas hydrate locations, I/Br ratios change rapidly from seawater values (I/Br = 0.0005) to values between 0.3 and 0.5 but remain quite constant for the sections where methane is present, demonstrating the parallel behavior of these two halogens. In contrast to most other hydrate sites, in the sections associated with iodine concentration maxima, iodine and bromine do not follow similar enrichment paths, resulting in strong increases in the I/Br ratios to values up to 0.8 at Site 1245 just above the BSR. A comparison between I/Br ratios at the site with the most pronounced maximum (Site 1245) to that with the least developed one (Site 1251) illustrates this observation (Fig. **F4**).

F4. Depth distribution of I/Br (mM/mM) ratios, p. 19.

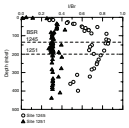

Iodine Isotope Ratios

A major goal of this investigation was the determination of ^{129}I/I ratios in the pore water. Because of the high concentrations in most of the samples, we were able to make AMS measurements on individual samples for this study. Although work on the halogen concentrations in pore water is completed, work on the iodine isotope ratios is still ongoing. We report here results for an initial set of samples, tabulated in Table **T2;** the study will be continued and further results will be reported in a separate paper. So far, we have measured 41 samples, with >1 sample from all sites except Site 1249. Although we have results for all of the sites, we have a somewhat complete profile only from Site 1245 at this time.

T2. Iodine isotopic compositions and minimum ages, p. 25.

All of the ratios are below the marine input ratio (R_i = [1500 ± 150] × 10^{-15}) (Moran et al., 1998), demonstrating the absence of contamination from anthropogenic sources (Fig. **F5**). The highest ratio (R_m = 760 × 10^{-15}; t_{min} = 15 Ma) was found for a shallow sample from Site 1244, but the majority of samples have ratios between 150 and 250 × 10^{-15}. Using equation 1, this range corresponds to minimum ages between 40 and 52 Ma for iodine in the pore water. For three sites (Sites 1244, 1245, and 1251), a sufficient number of samples was measured to construct depth profiles (Fig. **F6**). Error margins for individual samples are generally <20%, with some being as high as 78%. Although the error margins are somewhat larger than obtained for similar investigations (Fehn et al., 2000, 2003), the overall trends in these profiles are nevertheless clearly visible. In general, a decrease in ratios with depth is observed for the individual cores, although data coverage is too limited so far to indicate whether this decrease is monotonous or not. There are several samples at depths beyond 100 mbsf that have ratios higher than R_m = 400 × 10^{-15} (t_{min} = 30 Ma). The most complete depth profile available so far is for Site 1245. It indicates that there is at least one clearly defined maximum in the ^{129}I/I ratios, which reaches a value of R_m = 650 × 10^{-15} at a depth of 120 mbsf. The presence of this maximum is supported by the systematic increase of values above and below this depth. Although several of the other cores also show the presence of higher ^{129}I/I values, because of the limited data coverage it is too early to decide whether these higher values indicate systematic maxima as well.

F5. Summary plot of ^{129}I/I ratios, p. 20.

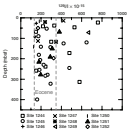

F6. Depth profiles of ^{129}I/I ratios, p. 21.

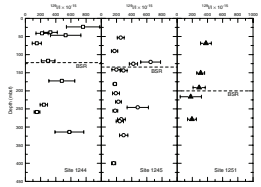

DISCUSSION

The pore fluids at Hydrate Ridge show the strongest enrichment in iodine observed at any gas hydrate site, consistent with the unusually high concentration of gas hydrates there. The biophilic behavior of iodine and the close association between iodine and methane observed here and at other gas hydrate areas suggest that methane and iodine are derived from the same organic material and travel together in aqueous fluids until they reach areas close to the seafloor (e.g., Fehn et al., in press). The ages found for the iodine in the pore water can thus be used to identify formations responsible for the release of the methane found in the gas hydrate.

All iodine ages found in pore water at Hydrate Ridge are older than 15 Ma. Because this age is considerably older than the ages of the shallow sediments hosting the gas hydrates, the pore water must contain iodine that was not locally derived. The majority of the samples have ratios between 150 and 250 $\times$ 10^{-15}, corresponding to ages between 40 and 52 Ma. These ages are minimum values because the calculation does not take into account the potential addition of fissiogenic ^{129}I, which is a function mainly of age and uranium concentration in the host formation. A correction for the presence of this component in the age range observed here and with uranium concentrations typical for marine sediments would increase the ages by ~5 m.y. (Fehn et al., 2000), shifting the proposed ages for the old component in the pore fluids into a range between 45 and 57 Ma. This age range is beyond the ages of the currently subducting sediments (<10 Ma) and the formations underlying Hydrate Ridge and suggests that fluids contributing to the current pore water come from formations of early Eocene age or older in the overriding wedge. Profiles presented by Snavely (1987) suggest the presence of formations with ages of early Eocene just to the west of the Siletz terrane, the crystalline backstop in the area. Because the closest formations of this age are found at distances of 40 km or more, fluids must have traveled considerable distances through the overriding wedge in order to reach their present location. Fluid flow models of active margins suggest that fluids can move along the décollement or fractures, with actual velocities depending strongly on the permeability and the mode of flow (e.g., Saffer and Bekins, 1998, 1999). Rates between 0.0007 and 0.043 m/yr were calculated for steady-state flow in subduction zones, reaching values up to 54 m/yr for transient periods (Saffer and Bekins, 1998). These rates suggest that transport of fluids from the Eocene formations in the accretionary complex to the Hydrate Ridge is possible within time frames of the age of the current subduction configuration. The new suggestion here is that the origin of iodine and methane is not from the subducting sediments but from the overriding wedge. Although it seems likely that the waters are also derived from this source, it is conceivable that waters expelled from the subducting sediments have come into contact with formations of Eocene age, where they picked up iodine and methane. The ubiquitous presence of fractures in the overriding wedge suggested by seismologic surveys (Snavely, 1987; Snavely and Wells, 1996) supports the suggestion that fluid flow can occur over great distances in this area, which might also involve transport from the suggested source region into the décollement, a preferred conduit for fluids. Transport of hydrocarbons over distances of this magnitude is common in oil reservoirs (e.g., Moran et al., 1995) and sedimentary basins (e.g., Person et al., 1996). Im-

proved information on age distribution and the presence of deep fractures would be needed in order to be more specific on the flow paths taken by these fluids and the role played by the décollement in this transport model.

The presence of a distinct maximum in iodine concentrations in the depth profile for Site 1245 (and perhaps at some other sites) is unique as far as gas hydrate sites and warrants further discussion. The younger ages coincide with the maximum in iodine concentrations, although the widths of the two maxima are somewhat different. If ratios are plotted vs. the reciprocal of concentration (Fig. F7), two trends are visible in the data set. Trend A indicates dilution of a component with high concentrations of iodine and low $^{129}I/I$ ratios with fluids of low concentration and high $^{129}I/I$ ratios. If this trend is extrapolated to the surface, mixing is indicated between an old, iodine-rich source (C_1 = 2.2 mM; R_1 = 150 × 10^{-15}) with waters in shallow sediments (C_2 = 0.5 mM; R_2 = 1500 × 10^{-15}). The concentration found for the Holocene component in this mixing pattern is within the range observed for fluids in shallow sediments (e.g., Martin et al., 1993; Egeberg and Dickens, 1999) and thus represents the contribution from recently deposited marine sediments. Although the "old" end-member used for this calculation is perhaps also affected by the presence of "young" material, the iodine concentration of the fluids with young material are relatively low so that their influence on the old end-member is negligible at the level of precision here. Trends similar to line A are observed also at other gas hydrate sites, as, for example, at Site 1230 (ODP Leg 201, Peru margin) (Fehn et al., in press).

F7. Mixing plot, Site 1245, p. 22.

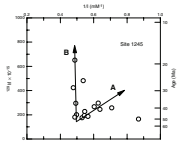

Trend B describes a line almost parallel to the y-axis, indicating mixing between two fluids with different iodine ages but quite similar iodine concentrations. Whereas the minimum age for the older source is close to that of trend A, the end point in the mixing plot for line B is at a sample with a ratio of 650 × 10^{-15}. The essentially vertical shape of the mixing line between the two end-members suggests that the mixing ratio here is close to 1:1 (Faure and Mensing, 2005). Assuming concentrations of 2.0 mM and equal contributions between the old and young member, we find a ratio of 1140 × 10^{-15} (corresponding to 6.2 Ma) for the young end-member. The actual age for the latter component is probably somewhat younger, however, because we cannot be sure that we found the exact maximum in the distribution of isotope ratios. Likely sources for the "young" material are the formations of Pliocene age underlying Hydrate Ridge (see Fig. F1B), although derivation from currently subducting sediments cannot be ruled out either.

I/Br ratios may also be used to indicate the presence of more than one source at several of the sites, specifically at the flank sites. A comparison to other gas hydrate sites (Egeberg and Dickens, 1999; Fehn et al., 2003) indicates that this ratio is always considerably elevated compared to seawater but is site specific, reaching quite constant values within a given site at depths beyond the influence of recent seawater. These ratios probably reflect the characteristics of the organic sources responsible for the addition of iodine and bromine to pore water. In the case of Hydrate Ridge, maxima in the depth distribution of iodine concentrations are accompanied by simultaneous maxima in I/Br ratios. This observation is in good agreement with the interpretation of $^{129}I/I$ results, indicating that the young high-I source also has higher I/Br ratios than the old high-I source.

The results of the iodine isotopes suggest that a major part of the iodine and methane in the pore water is not derived from local sources but from older formations at considerable distance from Hydrate Ridge. Indirect evidence for large-scale transport comes also from the freshening with depth of pore water observed at several sites, most clearly at the slope basin sites, which has been interpreted at sites such as the Nankai Trough as evidence for the addition of deep fluids (Kastner et al., 1993). A concurrent study of strontium isotopes at Hydrate Ridge might also show the presence of waters of Eocene age in several of the cores, most clearly discernable at the slope basin sites (R. Matsumoto, pers. comm., 2004), although these results have also been interpreted as the result of the interaction of waters with the basement (Torres et al., 2004; Teichert et al., in press).

CONCLUSIONS

Hydrate Ridge is the site of unusually high concentrations of gas hydrates. Pore water at Leg 204 sites shows the enrichment in iodine and bromine typical for gas hydrate sites, with the enrichment being somewhat higher than at other locations. Several of the cores display distinct maxima in iodine concentrations at the depths just above the BSR, a feature not observed in other gas hydrate sites. These maxima are most pronounced at the flank sites (e.g., Site 1245), but are absent from the slope basin sites (e.g., Site 1251). An initial set of $^{129}I/I$ ratios indicates the presence of iodine in all cores derived from organic sources with ages of ~50 Ma. The maxima found at several cores contain material derived from sources younger than 10 Ma.

The ages found here suggest that contributions from sources within the sediments hosting the gas hydrates constitute only a minor part of iodine and, by association, methane in Hydrate Ridge. A large fraction of the iodine is derived from sources with early Eocene ages. Potential source formations of this age are to be found in marine sediments of Eocene age located 40 km to the east. Pliocene formations underlying Hydrate Ridge also contribute, especially at the flank sites, and are probably responsible for the local maxima in iodine concentrations observed just above the BSR. Similar to results from other gas hydrate sites, the results indicate large-scale fluid transport and derivation of a major fraction of iodine and methane from sediments of Eocene age. The transport is probably driven by compaction and/or seismic pumping and is facilitated by the presence of multiple fractures in the Cascadia margin. Further iodine isotope data are needed in order to evaluate the causes of variations observed in iodine concentrations within the gas hydrate field of Hydrate Ridge and to relate them to potential differences in the hydrologic characteristics within the area.

ACKNOWLEDGMENTS

We are grateful to A. Tréhu and G. Bohrmann for the organization of Leg 204, to the shipboard party for providing the samples from this cruise, and to E. Gracia and the other organizers for the splendid postcruise conference in Barcelona. We thank G. Snyder for help during the sample preparation and Y. Muramatsu and R. Matsumoto for making unpublished data available. We appreciate the work by D. Elmore, M. Caffee, and colleagues on the ^{129}I determinations at PrimeLab, Purdue

University (West Lafayette, Indiana, USA). Thoughtful reviews by P. Santschi, M. Torres, and an anonymous reviewer are gratefully acknowledged. This research used samples and data provided by the Ocean Drilling Program (ODP). ODP is sponsored by the U.S. National Science Foundation (NSF) and participating countries under management of Joint Oceanographic Institutions (JOI), Inc. Funding for this research was provided by JOI-ODP F001703.

REFERENCES

Broecker, W.S., and Peng, T.-H., 1982. *Tracers in the Sea:* Palisades, NY (Eldigio Press).

Cooper, L.W., Beasley, T.M., Zhao, X.-L., Soto, C., Vinogradova, K.L., and Dunton, K.H., 1998. Iodine-129 and plutonium isotopes in arctic kelp as historical indicators of transport of nuclear fuel-reprocessing wastes from mid-to-high latitudes in the Atlantic Ocean. *Mar. Biol.,* 131:391–399.

Egeberg, P.K., and Dickens, G.R., 1999. Thermodynamic and pore water halogen constraints on gas hydrate distribution at ODP Site 997 (Blake Ridge). *Chem. Geol.,* 153:53–79.

Fabryka-Martin, J., Bentley, H., Elmore, D., and Airey, P.L., 1985. Natural iodine-129 as an environmental tracer. *Geochim. Cosmochim. Acta,* 49:337–347.

Faure, G., and Mensing, T.M., 2005. *Isotopes: Principles and Applications:* New Jersey (John Wiley & Sons).

Fehn, U., Holdren, G.R., Elmore, D., Brunelle, T., Teng, R., and Kubik, P.W., 1986. Determination of natural and anthropogenic I-129 in marine sediments. *Geophys. Res. Lett.,* 13:137–139.

Fehn, U., Peters, E.K., Tullai-Fitzpatrick, S., Kubik, P.W., Sharma, P., Teng, R.T.D., Gove, H.E., and Elmore, D., 1992. ^{129}I and ^{36}Cl concentrations in waters of the eastern Clear Lake area, California: residence times and source ages of hydrothermal fluids. *Geochim. Cosmochim. Acta,* 56:2069–2079.

Fehn, U., Snyder, G., and Egeberg, P.K., 2000. Dating of pore waters with I-129: relevance for the origin of marine gas hydrates. *Science,* 289:2332–2335.

Fehn, U., Snyder, G.T., Matsumoto, R., Muramatsu, Y., and Tomaru, H., 2003. Iodine dating of pore waters associated with gas hydrates in the Nankai area, Japan. *Geology,* 31:521–524.

Fehn, U., Snyder, G.T., and Muramatsu, Y, in press. Iodine as a tracer of organic material: ^{129}I results from gas hydrate systems and fore arc fluids. *J. Geochem. Explor.*

Frape, S.K., Blyth, A., Blomqvist, R., McNutt, R.H., and Gascoyne, M., 2004. Deep fluids in the continents. II. Crystalline rocks. *Treatise Geochem.,* 5:541–580.

Hesse R., 2003. Pore water anomalies of submarine gas-hydrate zones as tool to assess hydrate abundance and distribution in the subsurface—what have we learned in the past decade? *Earth-Sci. Rev.,* 61:149–179.

Jarrard, R.D., 1986. Relations among subduction parameters. *Rev. Geophys.,* 24:217–284.

Johnson, J.E., Goldfinger, C., and Suess, E., 2003. Geophysical constraints on the surface distribution of authigenic carbonates across the Hydrate Ridge region, Cascadia margin. *Mar. Geol.,* 202:79–120.

Kastner, M., Elderfield, H., Jenkins, W.J., Gieskes, J.M., and Gamo, T., 1993. Geochemical and isotopic evidence for fluid flow in the western Nankai subduction zone, Japan. *In* Hill, I.A., Taira, A., Firth, J.V., et al., *Proc. ODP, Sci. Results,* 131: College Station, TX (Ocean Drilling Program), 397–413.

Linde, D. (Ed.), 2005. *CRC Handbook of Chemistry and Physics (85th ed.), 2004–2005:* New York (CRC Press).

Martin, J.B., Gieskes, J.M., Torres, M., and Kastner, M., 1993. Bromide and iodine in Peru margin sediments and pore fluids: implication for fluid origins. *Geochim. Cosmochim. Acta,* 57:4377–4389.

Moran, J.E., Fehn, U., and Hanor, J.S., 1995. Determination of source ages and migration of brines from the U.S. Gulf Coast Basin using ^{129}I. *Geochim. Cosmochim. Acta,* 59:5055–5069.

Moran, J.E., Fehn, U., and Teng, R.T.D., 1998. Variations in $^{129}I/^{127}I$ ratios in recent marine sediments: evidence for a fossil organic component. *Chem. Geol.,* 152:193–203.

Moran, J.E., Oktay, S., and Santschi, P.H., 1999. Atmospheric dispersal of ^{129}iodine from nuclear fuel reprocessing facilities. *Environ. Sci. Tech.,* 33:2536–2542.

Muramatsu, Y., Fehn, U., and Yoshida, S., 2001. Recycling of iodine in fore-arc areas: evidence from the iodine brines of Chiba, Japan. *Earth Planet. Sci. Lett.,* 192:583–593.

Muramatsu, Y., and Wedepohl, K.H., 1998. The distribution of iodine in the Earth's crust. *Chem. Geol.,* 147:201–216.

Oktay, S.D., Santschi, P.H., Moran, J.E., and Sharma, P., 2000. The ^{129}iodine bomb pulse recorded in Mississippi River delta sediments: results from isotopes of I, Pu, Cs, Pb, and C. *Geochim. Cosmochim. Acta,* 64:989–996.

Oktay, S.D., Santschi, P.H., Moran, J.E., and Sharma, P., 2001. ^{129}I and ^{127}I transport in the Mississippi River. *Environ. Sci. Technol.,* 35:4470–4476.

Parsons, T., Tréhu, A.M., Luetgert, J.H., Miller, K., Kilbride, F., Wells, R.E., Fisher, M.A., Flueh, E., Brink, U.T., and Christensen, N.I., 1998. A new view into the Cascadia subduction zone and volcanic arc: implications for earthquake hazards along the Washington margin. *Geology,* 26:199–202.

Person, M., Raffensperger, J.P., Ge, S., and Garven, G., 1996. Basin-scale hydrogeologic modeling. *Rev. Geophys.,* 34:61–87.

Saffer, D.M., and Bekins, B.A., 1998. Episodic fluid flow in the Nankai accretionary complex: timescale, geochemistry, flow rates, and fluid budget. *J. Geophys. Res.,* 103:30351–30371.

Saffer, D.M., and Bekins, B.A., 1999. Fluid budgets at convergent plate margins: implications for the extent and duration of fault-zone dilation. *Geology,* 27:1095–1098.

Santschi, P.H., and Schwehr, K.A., 2004. $^{129}I/^{127}I$ as a new environmental tracer or geochronometer for biogeochemical or hydrodynamic processes in the hydrosphere and geosphere: the central role of organo-iodine. *Sci. Total Environ.,* 321:257–271.

Schink, D.R., Santschi, P.H., Corapcioglu, O., Sharma, P., and Fehn, U., 1995. ^{129}I in Gulf of Mexico waters. *Earth Planet. Sci. Lett.,* 135:131–138.

Schwehr, K.A., and Santschi, P.H., 2003. A sensitive determination of iodine species in fresh and sea water samples, including organo-iodine, using high performance liquid chromatography and spectrophotometric detection. *Anal. Chim. Acta,* 482:59–71.

Sharma, P., Bourgeois, M., Elmore, D., Granger, D., Lipschutz, M.E., Ma, X., Miller, T., Mueller, K., Rickey, G., Simms, P., and Vogt, S., 2000. PRIME Lab AMS performance, upgrades and research applications. *Nucl. Instr. Meth.,* B172:112–123.

Snavely, P.D., and Wells, R.E., 1996. Cenozoic evolution of the continental margin of Oregon and Washington. *In* Rogers, A.M. (Ed.), *Assessing Earthquake Hazards and Reducing Risk in the Pacific Northwest.* U.S. Geol. Survey Prof. Pap., 1560:161–182.

Snavely, P.D., Jr., 1987. Tertiary geologic framework, neotectonics, and petroleum potential of the Oregon-Washington continental margin. *In* Scholl, D.W., Grantz, A., and Vedder, J.G. (Eds.), *Geology and Resource Potential of the Continental Margin of Western North America and Adjacent Ocean Basins—Beaufort Sea to Baja California.* Circum-Pac. Counc. Energy Miner. Resour., Earth Sci. Ser., 6:305–336.

Snyder, G., and Fehn, U., 2004. Global distribution of ^{129}I in rivers and lakes: implications for iodine cycling in surface reservoirs. *Nucl. Instrum. Methods Phys. Res., Sect. B,* 223/224:579–586.

Snyder, G.T., Riese, W.C., Franks, S., Fehn, U., Pelzmann, W.L., Gorody, A.W., and Moran, J.E., 2003. Origin and history of waters associated with coal-bed methane: ^{129}I, ^{36}Cl, and stable isotope results from the Fruitland formation, CO and NM. *Geochim. Cosmochim. Acta,* 67:4529–4544.

Teichert, B.M.A., Eisenhauer, A., Bohrmann, G., Haase-Schramm, A., Bock, B., and Linke, P., 2003. U/Th systematics and ages of authigenic carbonates from Hydrate Ridge, Cascadia margin: recorders of fluid flow variations. *Geochim. Cosmochim. Acta,* 67:3845–3857.

Teichert, B.M.A., Torres, M.E., and Bohrmann, G., in press. Fluid sources, major fluid pathways and diagenetic reactions across an accretionary prism revealed by Sr and B concentrations and isotopes. *Earth Planet. Sci. Lett.*

Tomaru, H., Matsumoto, R., Lu, H.L., and Uchida, T., 2004. Geochemical process of gas hydrate formation in the Nankai Trough based on chloride and isotopic anomalies in interstitial water. *Resour. Geol.,* 54:45–51.

Torres, M.E., Teichert, B.M.A., Tréhu, A.M., Borowski, W.S., and Tomaru, H., 2004. Relationship of pore water freshening to accretionary processes in the Cascadia margin: fluid sources and gas hydrate abundance. *Geophys. Res. Lett.,* 31:L22305.

Tréhu, A.M., Torres, M.E., Moore, G.F., Suess, E., and Bohrmann, G., 1999. Temporal and spatial evolution of a gas-hydrate-bearing accretionary ridge on the Oregon continental margin. *Geology,* 27:939–942.

Tréhu, A.M., Bohrmann, G., Rack, F.R., Torres, M.E., et al., 2003. *Proc. ODP, Init. Repts.,* 204 [CD-ROM]. Available from: Ocean Drilling Program, Texas A&M University, College Station TX 77845-9547, USA.

Ussler, W., and Paull, C.K., 2001. Ion exclusion associated with marine gas hydrate deposits. *In* Paull, C.K., and Dillon, W.P. (Eds.), *Natural Gas Hydrates: Occurrence, Distribution, and Detection* (Vol. 124). Geophys. Monogr., 41–51.

Figure F1. A. Tectonic setting of the Cascadia margin and the location of Hydrate Ridge (Leg 204). **B.** Simplified west–east cross section through the Cascadia margin at 44°50′ , ~20 km north of Hydrate Ridge (after Snavely, 1987; Snavely and Wells, 1996).

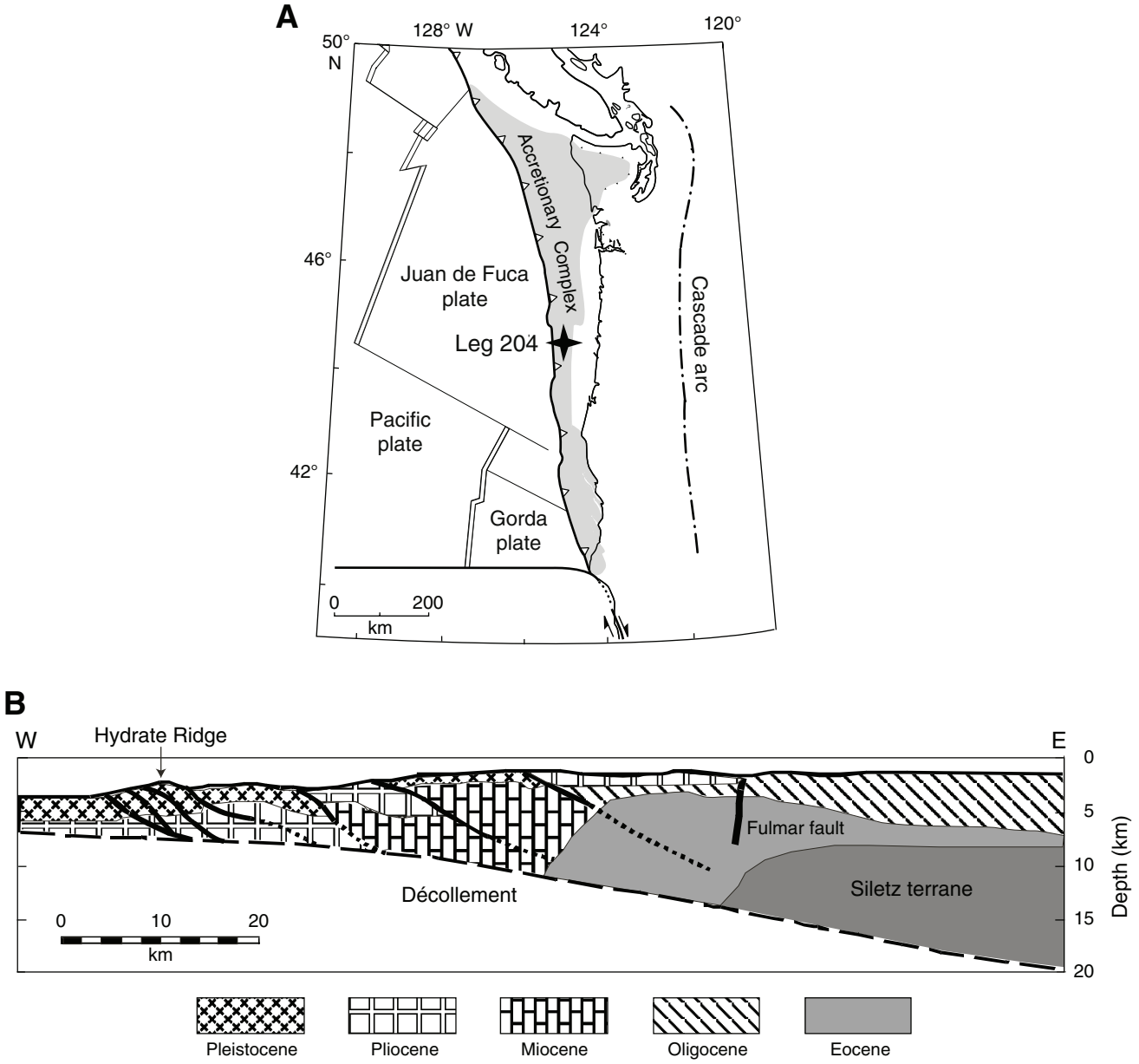

Figure F2. Distribution of drill sites during Leg 204. The sites are subdivided into flank (circles), summit (stars), and slope basin (diamonds).

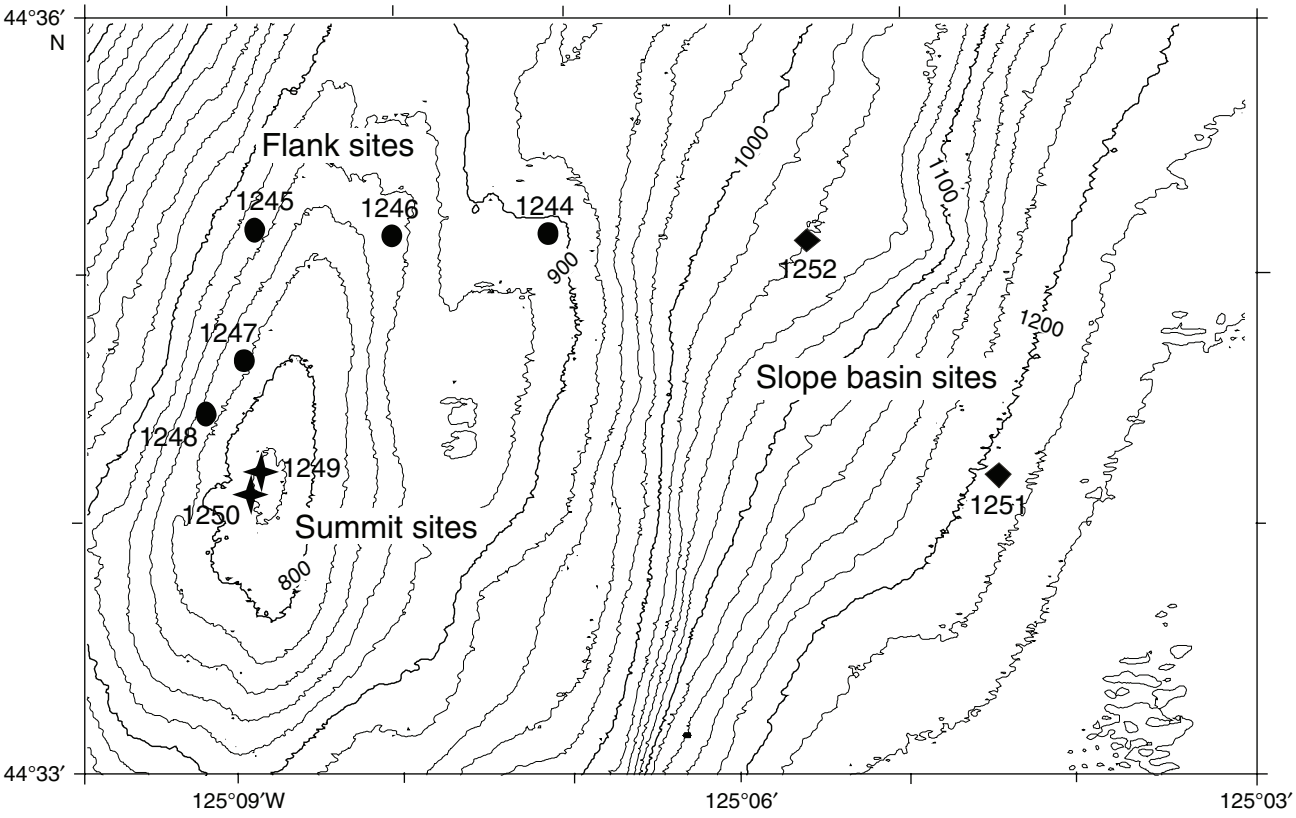

Figure F3. Depth profiles for concentrations of iodide, bromide, and chloride in Leg 204 sites. Broken lines = the depths of bottom simulating reflectors (BSRs). BSRs for Sites 1244 and 1246 are 10 and 20 m, respectively, above that of Site 1245; BSR for Site 1252 is 30 m above that of Site 1251.

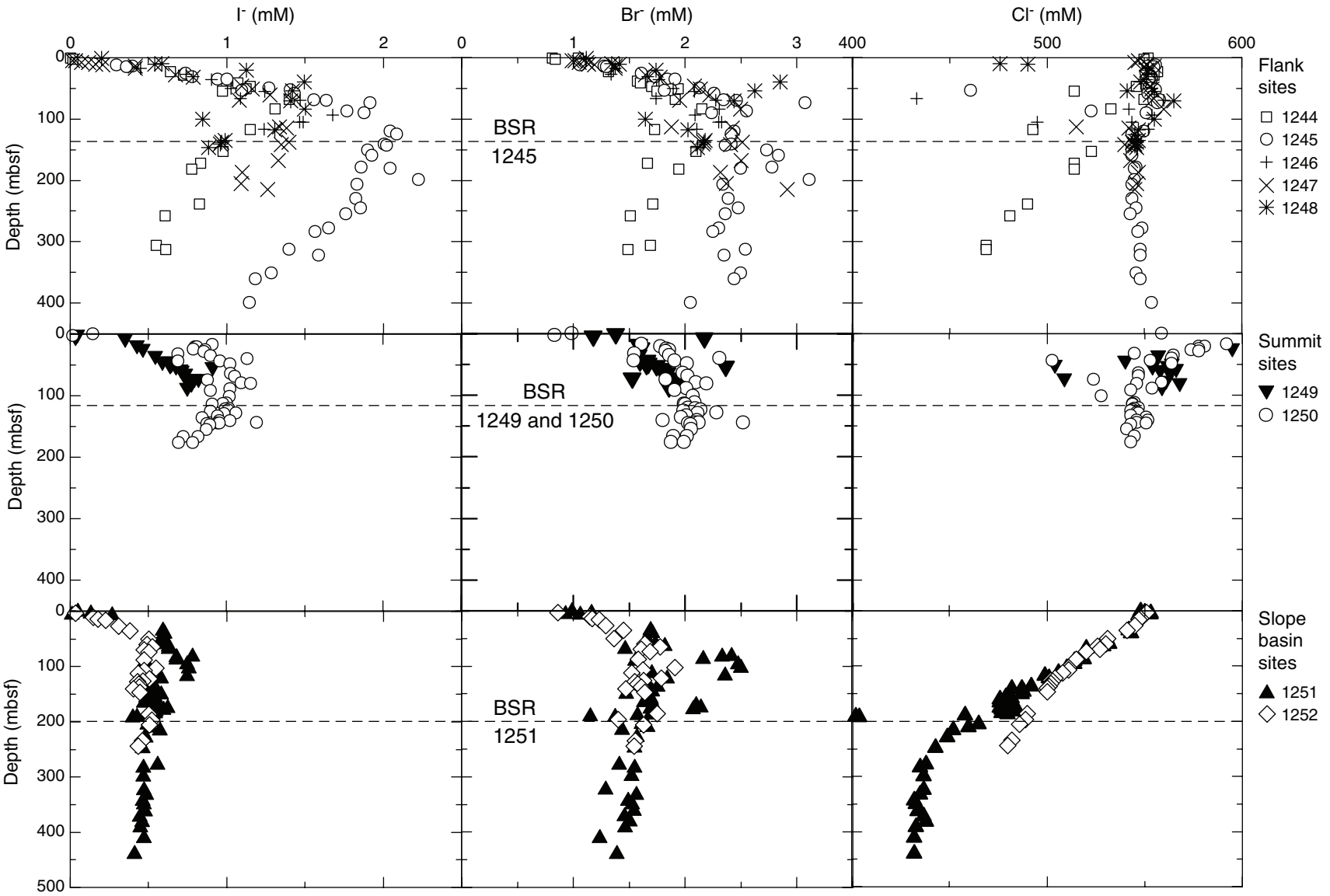

Figure F4. Depth distribution of I/Br (mM/mM) ratios in Sites 1245 and 1251. Whereas the profile for the slope basin Site 1251 reaches constant values with depth, a pronounced maximum in I/Br ratios is visible at flank Site 1245 just above the bottom simulating reflector (BSR).

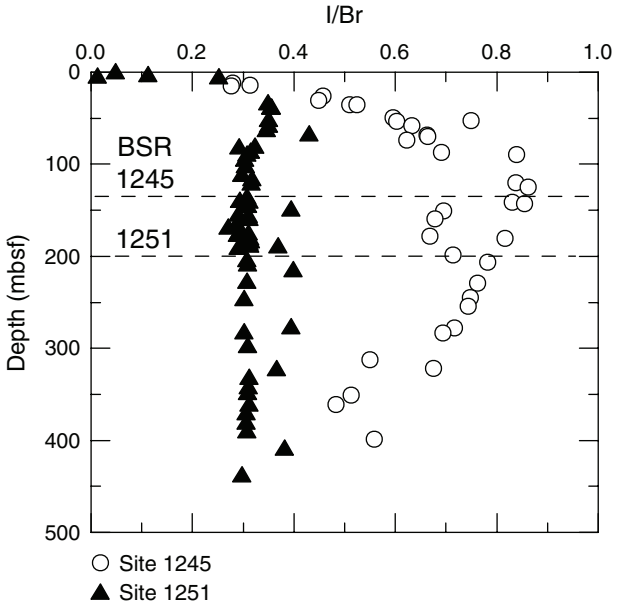

Figure F5. Summary plot of ^{129}I/I ratios in pore water from Leg 204. Most results fall into the Eocene age range, indicated by the vertical lines.

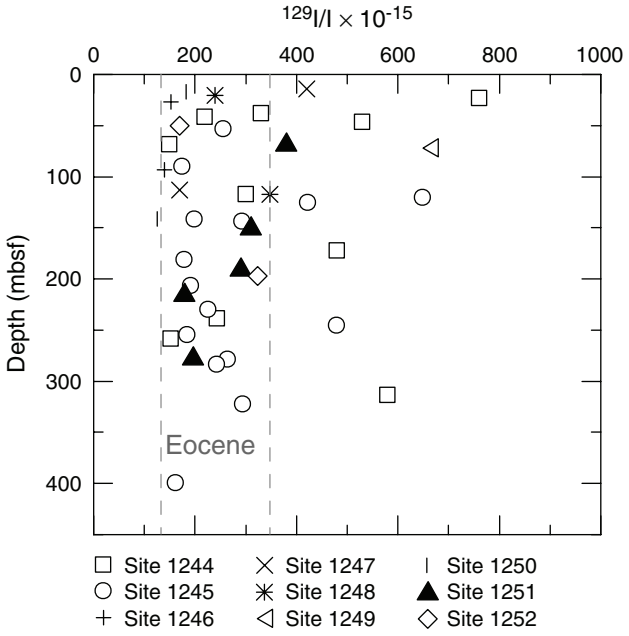

Figure F6. Depth profiles of ^{129}I/I ratios for Sites 1244, 1245, and 1251. The maximum in ^{129}I/I ratios observed in Site 1245 is just above the bottom simulating reflector (BSR), coinciding with the maximum in iodine concentrations at that site.

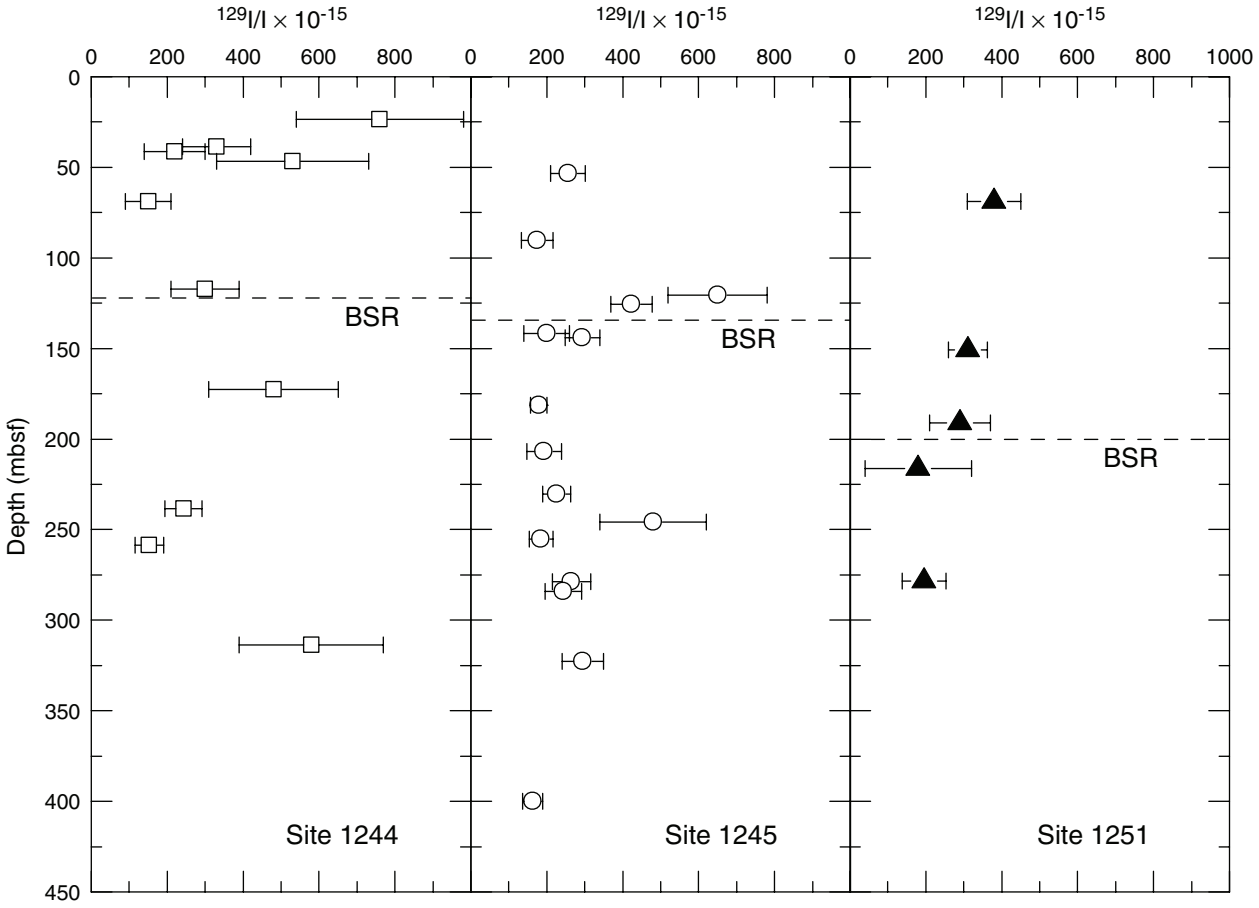

Figure F7. Mixing plot for Site 1245. Ages calculated using equation 1 are indicated on the right-hand axis. See text for discussion of the two trend lines identified in this diagram.

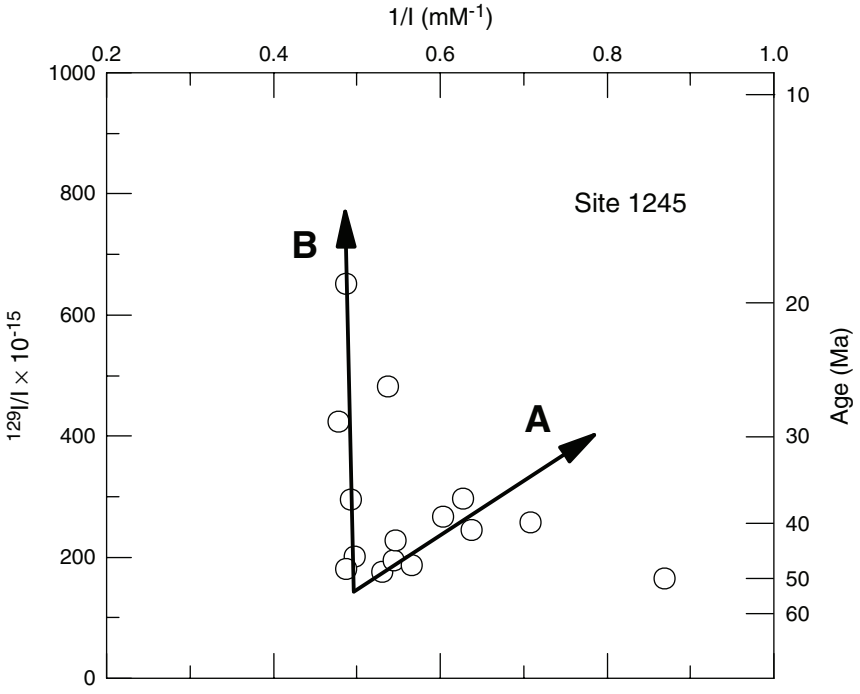

Table T1. Concentrations of iodine, bromine, and chlorine in pore water from Hydrate Ridge (ODP Leg 204). (See table note. Continued on next page.)

Hole, core	Depth (mbsf)	I (mM)	Br (mM)	Cl (mM)
204-				
1244B-1H	1.40	0.0038	0.8135	552
1244C-1H	1.40	0.0039	1.0458	NA
1244C-1H	2.90	0.0171	0.8385	550
1244B-3H	23.50	0.6425	1.3141	557
1244B-4H	28.63	0.7261	1.6058	555
1244B-5H	38.46	1.0000	1.5770	552
1244C-5H	41.35	1.0709	1.6020	554
1244B-5H	42.90	NA	NA	550
1244B-6H	46.78	1.1496	1.7021	546
1244B-6H	51.28	1.1260	1.9424	552
1244C-7H	54.79	0.9732	1.7497	514
1244C-8H	68.87	1.4016	1.9149	550
1244C-10H	83.55	1.3110	2.1527	533
1244C-13H	117.35	1.1496	1.7272	493
1244C-20X	153.55	0.9772	2.0989	523
1244C-22X	172.65	0.8346	1.6646	514
1244C-23X	182.25	0.7768	1.9462	514
1244C-29X	238.56	0.8268	1.7146	490
1244C-31X	258.60	0.6063	1.5144	481
1244C-36X	306.90	0.5522	1.6896	469
1244C-37X	313.50	0.6118	1.4894	469
1245B-2H	12.40	0.2992	1.0638	556
1245C-2H	14.90	0.4014	1.2778	552
1245B-2H	15.40	0.3618	1.3016	555
1245C-4H	26.40	0.7394	1.6108	551
1245B-4H	31.40	0.7802	1.7322	554
1245B-4H	35.90	0.9441	1.8473	554
1245C-5H	35.90	1.0063	1.9161	553
1245B-6H	50.40	1.2709	2.1302	554
1245B-6H	53.40	1.4094	1.8773	556
1245B-6H	54.28	1.0976	1.8185	461
1245B-7H	58.95	1.4346	2.2653	552
1245B-8H	69.32	1.5591	2.3467	558
1245B-8H	70.82	1.6386	2.4656	555
1245C-10H	74.48	1.9181	3.0763	557
1245B-10H	88.03	1.7709	2.5557	523
1245C-12H	90.25	1.8819	2.2403	551
1245C-16P	120.62	2.0472	2.4406	550
1245B-14H	125.45	2.0866	2.4155	544
1245B-16X	141.80	2.0079	2.4155	545
1245C-20X	143.95	2.0236	2.3655	544
1245B-18X	151.73	1.9039	2.7359	544
1245B-19X	159.75	1.9283	2.8385	544
1245B-21X	178.77	1.8606	2.7797	546
1245B-21X	181.27	2.0472	2.5031	545
1245C-28H	199.20	2.2299	3.1164	545
1245B-24X	206.95	1.8346	2.3404	544
1245B-26X	230.33	1.8268	2.3905	544
1245B-28X	245.68	1.8583	2.4781	546
1245B-29X	255.35	1.7638	2.3655	543
1245B-31X	278.76	1.6535	2.3029	549
1245B-32X	284.25	1.5669	2.2528	547
1245B-36X	313.50	1.4008	2.5407	548
1245B-37X	322.75	1.5906	2.3529	548
1245B-40X	351.65	1.2866	2.4994	546
1245B-41X	361.50	1.1843	2.4443	548
1245B-45X	399.85	1.1496	2.0526	554
1246B-3H	17.10	0.4493	1.3730	552
1246B-4H	26.60	0.7402	1.3392	552
1246B-4H	31.10	0.7844	1.6633	555
1246B-5H	36.10	0.9016	1.7672	551
1246B-6H	50.00	1.0268	1.8924	554
1246B-7H	54.89	1.2409	2.0814	555
1246B-8H	66.20	1.0882	1.7409	433
1246B-8H	69.10	1.4693	2.2716	560
1246B-10H	83.60	1.5016	2.3066	542
1246B-11H	93.10	1.6772	2.0901	554
1246B-12H	104.87	1.4669	2.2979	495
1246B-12H	105.47	1.4874	2.3267	543.5
1246B-13H	116.55	1.2402	2.1064	552
1247B-2H	4.34	0.0133	0.9876	547
1247B-2H	5.10	0.0353	1.0161	547
1247B-2H	8.00	0.0708	1.0516	545
1247B-2H	8.10	0.1178	1.1199	545
1247B-2H	10.34	0.1607	1.1350	551
1247B-2H	11.10	0.2079	1.1881	551
1247B-3H	13.84	0.4144	1.3742	555
1247B-3H	17.60	0.4144	1.3742	553
1247B-5H	27.50	0.6718	1.6458	NA
1247B-5H	31.34	0.7839	1.7760	551
1247B-7H	45.79	1.0961	2.0839	553
1247B-7H	50.95	1.1622	2.1352	554
1247B-8H	60.50	1.2756	2.2228	553
1247B-9H	69.29	1.0819	1.9512	554
1247B-11H	84.11	1.4937	2.4969	560
1247B-14H	113.00	1.3386	1.8773	515
1247B-15X	114.34	1.3835	2.4218	542
1247B-19X	137.37	1.3976	2.5094	544
1247B-19X	141.31	1.3496	2.4080	540
1247B-22X	167.24	1.3307	2.5019	543
1247B-24X	186.91	1.0992	2.3141	547
1247B-26X	205.55	1.0898	2.3667	546
1247B-27X	214.94	1.2622	2.9124	545
1248B-1H	1.20	0.1992	1.1176	NA
1248B-2H	9.16	0.5849	1.3442	476
1248C-2X	10.68	0.5409	1.4143	490
1248C-3X	20.60	1.1260	1.7397	551
1248C-5X	39.80	1.4969	2.8486	548
1248C-6H	53.84	1.4189	2.6220	541
1248C-8H	69.87	1.4102	2.4368	565
1248C-11H	100.36	0.8472	1.6421	555
1248C-13H	117.33	1.3071	2.0275	547
1248C-14H	125.62	NA	NA	545
1248C-15H	135.30	0.9906	2.1765	547
1248C-16H	137.85	0.9677	2.1677	546
1248C-16H	140.85	0.9575	2.1577	545
1248C-17X	143.35	NA	NA	545
1248C-17X	146.35	0.8850	2.1089	546
1249C-1H	0.00	0.0446	1.3817	778
1249C-2H	3.55	0.0346	1.1765	733
1249C-3H	6.96	0.3524	2.1740	1008
1249C-4H	17.61	0.4272	1.5870	618
1249F-7H	23.41	0.4659	1.6058	595
1249B-3A	34.71	0.5431	1.5832	557
1249F-9H	43.61	0.6261	1.6621	540
1249B-5A	44.18	0.5904	1.5982	554
1249C-8H	47.64	0.6474	1.6708	564
1249C-8H	50.18	0.6391	1.6558	504
1249F-10H	52.09	0.6788	1.7434	562
1249B-7A	52.82	0.9134	2.3655	554
1249C-9H	56.83	0.7057	1.8135	566
1249C-9H	58.18	0.7144	1.7947	558
1249F-12H	63.20	0.7377	1.8423	563
1249C-11H	71.74	0.8189	1.5269	509
1249C-11H	71.74	0.7929	1.9524	509
1249C-12H	75.70	0.7530	1.8598	561
1249F-15H	79.57	0.7737	1.8798	568
1249C-13H	86.29	0.7497	1.8536	559
1250C-1H	0.00	0.1464	0.9907	559
1250E-1H	2.81	0.0203	0.8329	NA
1250C-3H	16.90	0.9134	1.6145	592
1250D-3H	21.02	0.8031	1.7810	578
1250C-3H	21.40	0.8126	1.7810	581
1250D-3H	24.90	0.7921	1.8360	578
1250C-4H	26.40	0.8677	1.8598	574

Table T1 (continued).

Hole, core	Depth (mbsf)	I (mM)	Br (mM)	Cl (mM)
1250C-4H	29.00	0.8598	1.8273	578
1250D-4H	32.90	0.6927	1.5482	545
1250C-5H	35.88	0.9016	1.8586	565
1250C-5H	40.31	1.1339	2.3116	564
1250D-6H	44.24	0.6936	1.5419	553
1250C-6H	44.57	0.9606	1.9061	503
1250C-6H	48.95	1.0236	2.0200	564
1250C-8H	64.40	1.0291	1.9825	547
1250C-8H	68.90	1.0535	2.0275	547
1250C-10H	75.31	0.8811	1.8273	524
1250C-10H	79.81	1.0984	2.1001	559
1250D-10H	81.22	1.1591	2.1927	546
1250C-11H	89.31	1.0236	2.0163	554
1250C-12H	92.50	0.8984	1.9099	543
1250F-1H	101.55	1.0220	2.0738	528
1250F-2H	112.30	1.0024	2.0901	545
1250C-14H	113.80	0.9795	1.9912	544
1250F-3X	114.80	0.9102	2.0063	544
1250D-15X	120.91	1.0157	2.0313	547
1250F-5H	122.30	0.9929	2.0951	545
1250F-5H	123.80	1.0142	2.1389	544
1250C-15H	125.86	0.9016	1.9900	543
1250F-6X	128.60	1.0638	2.2816	546
1250F-6X	129.60	0.9882	2.1126	547
1250C-17H	133.30	0.9449	2.0138	543
1250C-17H	136.30	0.8457	1.9650	551
1250F-9X	141.30	0.9575	2.1089	552
1250C-19X	141.30	1.0236	1.8023	546
1250D-19X	144.50	1.1969	2.5194	NA
1250C-19X	145.00	0.8780	2.0300	551
1250F-10X	147.90	0.8976	2.0501	543
1250F-11X	155.68	0.8740	2.0563	541
1250F-12X	167.05	0.7272	1.8974	545
1250F-12X	167.05	0.8220	2.0213	545
1250F-13X (A)	176.65	0.6944	1.8748	543
1250F-13X (B)	176.65	0.7882	1.9950	543
1251E-1H	1.40	0.0482	0.9871	548
1251E-1H	2.90	NA	NA	550
1251E-1H	4.40	0.1317	1.1648	553
1251E-1H	5.90	0.0123	0.9307	553
1251B-1H	7.45	0.2677	1.0638	547
1251B-4H	35.50	0.5917	1.6921	542
1251B-5H	40.41	0.6060	1.7084	543
1251B-5H (R)	40.41	0.6016	1.6884	543
1251B-6H	53.61	0.5819	1.6633	531
1251B-7H	59.50	0.6069	1.7322	532
1251B-7H	64.00	0.6306	1.8198	529
1251B-8H	69.00	0.6299	1.4643	520
1251D-11H	82.29	0.7806	2.4168	NA
1251D-11H	83.06	0.6805	2.3317	518
1251B-10H	88.00	0.6794	2.1602	519
1251B-10H	91.00	0.4794	1.5557	514
1251B-11H	96.84	0.7496	2.4718	514
1251D-13H	103.67	0.7608	2.5006	510
1251B-13H	112.85	0.5067	1.7009	506
1251B-14H	117.91	0.7496	2.3579	499
1251D-15H	122.40	0.5827	1.8411	501
1251B-16H	137.40	0.5407	1.7572	492
1251D-17H	141.40	0.4954	1.6884	487
1251B-16H	141.81	0.5198	1.6671	482
1251B-17H	146.90	0.5283	1.7059	488
1251B-17H	150.90	0.5827	1.4768	487
1251D-19H	156.31	0.4865	1.6746	479
1251B-19H	158.16	0.5255	1.6896	482
1251D-19H	160.81	0.5294	1.6971	476
1251B-19H	161.08	0.5267	1.6859	480
1251D-20H	166.13	0.4709	1.6358	476
1251B-20H	170.48	0.5697	2.1001	482
1251B-22H	175.50	0.6239	2.1402	476
1251D-22X	176.87	0.5253	1.6896	478
1251B-22H	178.48	0.5972	2.0701	477
1251D-23X	181.82	0.5461	1.7459	484
1251D-23X	182.32	0.5315	1.7096	485
1251B-23H	185.00	0.5438	1.7309	477
1251B-23H	187.72	0.5297	1.6946	480
1251D-24X	189.62	0.4931	1.5732	458
1251D-24X	191.12	0.4252	1.1514	402
1251D-24X	192.52	0.4002	1.3767	404
1251D-25X	205.45	0.4958	1.6133	465
1251D-26X	210.43	0.5137	1.6646	460
1251B-27X	216.25	0.5748	1.4393	452
1251B-28X	228.85	0.4821	1.5682	449
1251B-30X	248.00	0.4663	1.5469	443
1251B-33X	278.55	0.5591	1.4143	438
1251B-34X	283.78	0.4679	1.5507	435
1251B-36X	299.40	0.4700	1.5207	437
1251B-39X	324.20	0.4724	1.2891	437
1251B-41X	333.40	0.4885	1.5632	435
1251B-42X	343.50	0.4630	1.4919	432
1251B-43X	350.43	0.4724	1.5294	433
1251B-44X	362.70	0.4813	1.5457	434
1251B-45X	372.30	0.4469	1.4618	437
1251B-46X	381.90	0.4620	1.5056	438
1251B-47X	391.60	0.4500	1.4643	433
1251B-50X	410.80	0.4724	1.2390	432
1251B-53X	439.78	0.4130	1.3905	432
1252A-1H	2.85	0.0332	0.8636	551
1252A-2H	10.75	0.1480	1.1471	NA
1252A-2H	13.75	0.1786	1.1677	548
1252A-3H	16.00	0.2257	1.2325	547
1252A-4H	26.75	0.3101	1.2879	545
1252A-5H	35.34	0.3822	1.4481	541
1252A-6H	50.25	0.5039	1.3642	531
1252A-7H	59.75	0.4919	1.6395	530
1252A-8H	64.75	0.5240	1.7747	526
1252A-8H	69.25	0.4734	1.6058	527
1252A-9H	74.25	0.5006	1.6846	520
1252A-10H	87.35	0.4708	1.5832	515
1252A-12H	102.75	0.5468	1.9086	511
1252A-12H	107.15	0.4705	1.6208	511
1252A-13H	112.25	0.4359	1.5219	508
1252A-14H	121.75	0.5069	1.7847	504
1252A-15X	125.84	0.4646	1.6308	502
1252A-15X	127.85	0.4300	1.5494	503
1252A-15X	132.18	0.4372	1.5757	502
1252A-16X	137.50	0.4403	1.6083	501
1252A-16X	140.50	0.4033	1.4706	500
1252A-17X	147.20	0.4467	1.6408	500
1252A-21X	185.90	0.5004	1.7497	490
1252A-22X	197.00	0.5197	1.4018	489
1252A-23X	205.78	0.5044	1.6295	486
1252A-26X	234.80	0.4597	1.5519	482
1252A-27X	244.50	0.4342	1.5444	480

Note: NA = not analyzed.

Table T2. Iodine isotopic compositions and minimum ages in pore water from ODP Leg 204.

Hole, core	Depth (mbsf)	$^{129}I/I \times 10^{-15}$	±	Age (Ma)
204-				
Flank sites				
1244B-3H	23.5	760	220	15
1244B-5H	38.46	330	90	34
1244C-5H	41.35	220	80	44
1244B-6H	46.78	530	200	24
1244C-8H	68.87	150	60	52
1244C-13H	117.35	300	90	36
1244C-22X	172.65	480	170	26
1244C-29X	238.56	243	49	41
1244C-31X	258.6	153	38	52
1244C-37X	313.5	580	190	22
1245B-6H	53.4	256	46	40
1245C-12H	90.25	175	42	49
1245C-16P	120.62	650	130	19
1245B-14H	125.45	423	55	29
1245B-16X	141.8	200	60	46
1245C-20X	143.95	294	45	37
1245B-21X	181.27	179	22	48
1245B-24X	206.95	193	45	46
1245B-26X	230.33	226	37	43
1245B-28X	245.68	480	140	26
1245B-29X	255.35	185	31	47
1245B-31X	278.76	265	51	39
1245B-32X	284.25	244	48	41
1245B-37X	322.75	295	55	37
1245B-45X	399.85	163	26	50
1246B-4H	26.6	153	56	52
1246B-11H	93.1	140	29	54
1247B-3H	13.84	420	100	29
1247B-14H	113	170	23	49
1248C-3X	20.6	240	60	42
1248C-13H	117.33	348	55	33
Summit sites				
1249C-11H	71.74	670	90	18
1250C-3H	16.9	182	49	48
1250C-19X	141.3	126	40	56
Basin sites				
1251B-8H	69	380	70	31
1251B-17H	150.9	311	51	36
1251D-24X	191.12	290	80	37
1251B-27X	216.25	180	140	48
1251B-33X	278.55	196	58	46
1252A-6H	50.25	170	90	49
1252A-22X	197	323	50	35